Metal Dependence of the Contributions of Low-Frequency Normal Coordinates to the Sterically Induced Distortions of Meso-Dialkyl-Substituted Porphyrins

Xing-Zhi Song,[†,‡] Laurent Jaquinod,[§] Walter Jentzen,[†] Daniel J. Nurco,[§] Song-Ling Jia,[†,‡] Richard G. Khoury,[§] Jian-Guo Ma,[†,‡] Craig J. Medforth,[§] Kevin M. Smith,[§] and John A. Shelnutt*[,†,‡]

Materials Theory and Computation Department, Sandia National Laboratories,[||] Albuquerque, New Mexico 87185-1349, Department of Chemistry, University of New Mexico, Albuquerque, New Mexico 87131, and Department of Chemistry, University of California,[⊥] Davis, California 95616

Received April 24, 1997

The influence of central metals of different sizes on the macrocyclic structure of a series of 5,15-disubstituted metalloporphyrins has been investigated with X-ray crystallography, molecular mechanics (MM) calculations, and resonance Raman spectroscopy. MM calculations indicate that the series of porphyrins are in a gabled (*gab*) conformation consisting of a linear combination of *ruf* (B_{1u}) and *dom* (A_{2u}) out-of-plane normal-coordinate deformation types. The MM-calculated *gab* structures have been structurally decomposed into equivalent displacements along the lowest-frequency normal coordinate of each symmetry type. The contributions of each normal coordinate to the total distortion agree well with the contributions obtained from normal-coordinate structural decomposition of the X-ray crystal structures. Symmetry considerations show that any relative proportion of the *ruf* and *dom* deformations is allowed in the *gab* distortion. Varying the size of the central metal causes a change in the ratio of the *dom*/*ruf* contributions. A large metal like zinc disfavors ruffling over doming, significantly reducing the ruffling contribution and slightly increasing the doming contribution. In addition, the total degree of nonplanar distortion is reduced for large metals. This is confirmed for the series of disubstituted metalloporphyrins by smaller downshifts of the structure-sensitive Raman lines for the larger metals.

Introduction

There is growing acceptance of the possible functional significance of the nonplanar conformational distortions seen for tetrapyrroles in biological systems.[1] Nonplanar distortions of the tetrapyrrole macrocycles in heme-containing proteins have been observed in various X-ray crystal structures.[2] For example, the crystal structures of mitochondrial cytochromes *c* display a large nonplanar distortion which was subsequently shown to be conserved in cytochromes *c* from several species.[3,4] The importance of this observation is enhanced by the discovery that the heme can only be nonplanar at considerable energy expense to the protein matrix.[5] This work forms part of a growing body of research in both biological systems and highly nonplanar model porphyrin systems demonstrating the profound effect that nonplanar distortions can have on the chemical and photophysical properties of porphyrins and metalloporphyrins.[6]

Recently, we have observed that nonplanar distortions for a symmetrically substituted metalloporphyrin often occur along only one of the lowest-frequency out-of-plane normal coordinates of the macrocycle (B_{1u} *ruf*, B_{2u} *sad*, A_{2u} *dom*, and E_g *wav*), called normal deformations.[7] For an asymmetrically substituted porphyrin or a porphyrin in a protein, the more complicated nonplanar distortion may be represented in terms of a linear

* To whom correspondence should be addressed.
[†] Sandia National Laboratories.
[‡] University of New Mexico.
[§] University of California.
[||] Sandia is a multiprogram laboratory operated by Sandia Corporation, a Lockheed Martin Company, for the United States Department of Energy under Contract DE-AC04-94AL85000 (J.A.S.).
[⊥] Work performed at the University of California at Davis was supported by grants from the National Science Foundation (CHE-93-05577) and the National Institutes of Health (HL-22252) (K.M.S.).

(1) (a) Longa, S. D.; Ascone, I.; Fontaine, A.; Castellano, A. C.; Bianconi, A. *Eur. Biophys. J.* **1994**, *23*, 361. (b) Haggin, J. *Chem. Eng. News* **1991**, Jan 14, 23. (c) Ravikanth, M.; Reddy, D.; Chandrashekar, T. K. *Chem. Phys. Lett.* **1994**, *222*, 563. (d) Maiti, W. C.; Ravikanth, M. *J. Chem. Soc., Faraday Trans.* **1996**, *92*, 1095. (e) Tetreau, C.; Lavalette, D.; Momenteau, M.; Fisher, J.; Weiss, R. *J. Am. Chem. Soc.* **1994**, *116*, 11840. (f) Gentemann, S.; Medforth, C. J.; Ema, T.; Nelson, N. Y.; Smith, K. M.; Fajer, J.; Holten, D. *Chem. Phys. Lett.* **1995**, *245*, 441. (g) Shelnutt, J. A.; Song, X.-Z.; Ma, J.-G.; Jia, S.-L.; Jentzen, W.; Medforth, C. J. *Chem. Soc. Rev.* **1998**, *27*, 31.
(2) (a) Kratky, C.; Waditschatka, R.; Angst, C.; Johansen, J.; Plaquevent, J. C.; Schreiber, J.; Eschenmoser, A. *Helv. Chim. Acta* **1982**, *68*, 1312. (b) Waditschatka, R.; Kratky, C.; Jaun, B.; Heinzer, J.; Eschenmoser, A. *J. Chem. Soc., Chem. Commun.* **1985**, 1604. (c) Geno, M. K.; Halpern, J. *J. Am. Chem. Soc.* **1987**, *109*, 1238. (d) Furenlid, L. R.; Renner, M. W.; Smith, K. M.; Fajer, J. *J. Am. Chem. Soc.* **1990**, *112*, 1634.
(3) (a) Berghuis, A. M.; Brayer, G. D. *J. Mol. Biol.* **1992**, *223*, 959. (b) Martinez, S. E.; Smith, J. L.; Huang, D.; Szczepaniak, A.; Cramer, W. A. In *Reseach in Photosynthesis*; Murata, N., Ed.; Proceedings of the IXth International Congress on Photosynthesis; Kluwer Academic: Dordrecht, The Netherlands, 1992; Vol. 2, p 495.
(4) Hobbs, J. D.; Shelnutt, J. A. *J. Protein Chem.* **1995**, *14*, 19.
(5) Anderson, K. K.; Hobbs, J. D.; Luo, L.; Stanley, K. D.; Quirke, J. M. E.; Shelnutt J. A. *J. Am. Chem. Soc.* **1993**, *115*, 12346.
(6) (a) Barkigia, K. M.; Chantranupong, L.; Smith, K. M.; Fajer, J. *J. Am. Chem. Soc.* **1988**, *110*, 7566. (b) Kadish, K. M.; Van Caemelbecke, E. V.; D'Souza, F. D.; Medforth, C. J.; Smith, K. M.; Tabard, A. *Organometallics* **1993**, *12*, 2411. (c) Kadish, K. M.; Van Caemelbecke, E. V.; Boulas, P.; D'Souza, F. D.; Vogel, E.; Kisters, M.; Medforth, C. J.; Smith, K. M. *Inorg. Chem.* **1993**, *32*, 4177. (d) Gudowska-Nowak, E.; Newton, M. D.; Fajer, J. *J. Phys. Chem.* **1990**, *94*, 5795. (e) Medforth, C. J.; Berber, M. D.; Smith, K. M.; Shelnutt, J. A. *Tetrahedron Lett.* **1990**, *31*, 3719.

S0020-1669(97)00465-5 CCC: $15.00
Published on Web 04/01/1998

combination of displacements along these lowest-frequency normal deformations.[8] To test this notion, the normal-coordinate structural decomposition method has been used to analyze the out-of-plane deformations of the hemes contained in X-ray crystal structures of proteins.[9] The decomposition results reveal previously hidden influences of the protein on the conformation of the heme. In many cases, the conformations of the hemes are conserved within proteins that belong to a single functional group. These include cytochromes *c*, c_3, c′, and P450 and the peroxidases.[10] The influences of the refinement method, the crystallization conditions, and the research group carrying out the X-ray structure determination were ascertained for the hemes contained in hemoglobin. The hemes in the α- and β-chains of human deoxyhemoglobin A crystal structures show α/β differences, but are similar within each subunit. Specifically, the distortion of the α-hemes is primarily *dom* and *ruf*, while the distortion of the hemes in the β-chains is *sad* and *dom*.[9]

In order to investigate the roles of these different types of nonplanar distortions in biological processes, it is useful to design and study models of metalloporphyrins that have conformations similar to those of the proteins. Previous studies have shown that the type and degree of nonplanar deformation can be controlled by the peripheral substitution pattern, the steric bulkiness of substituents, and the size of the central metal of the macrocycle.[8,11] In this vein, the investigation of a series of nickel(II) meso-tetrasubstituted porphyrins has more fully characterized the pure *ruf* distortion as a model for the conserved ruffling of the heme of cytochromes *c*.[7] We have also shown that the conformations of a series of nickel(II) 5,15-disubstituted porphyrins consist of both ruffling and doming. Thus, these disubstituted porphyrins serve as a model for the ruffling and doming in the hemes of the α-chains of human deoxyhemoglobin A.[8] The series of nickel(II) 5,15-disubstituted porphyrins (Figure 1) were found to adopt a gabled (*gab*) or roof conformation of the macrocycle.[8] In this conformation, the porphyrin ring is folded about a line through the two opposite bridging meso carbons that possess the alkyl substituents. This *gab* distortion was shown to be composed of a linear combination of distortions along the lowest-frequency out-of-plane macrocyclic normal coordinates of B_{1u} (*ruf*) and A_{2u} (*dom*) symmetry types. As the substituents became more bulky [in the order phenyl (P), propyl (Pr), isopropyl (iPr) and *tert*-butyl (tBu)], the degree of gabling distortion increases.

We now extend our systematic study of the 5,15-disubstituted porphyrins to an investigation of the metal dependence of these nonplanar deformations. The series of metal porphyrins for which the ionic radius of the metal and the optimum metal−nitrogen bond length increase within the metal series [nickel(II), cobalt(II), copper(II), and zinc(II)] is investigated using X-ray crystallography, molecular mechanics calculations, and resonance Raman spectroscopy. The relative contributions of the *ruf* and *dom* deformations in the crystal structures of several metal complexes of the 5,15-disubstituted porphyrins are found to be metal-dependent in a fashion that is accurately predicted by molecular modeling. The results obtained also demonstrate the *quantitative* validity of normal-coordinate structural decomposition when only the lowest-frequency coordinate of each symmetry type is used to describe the structure.

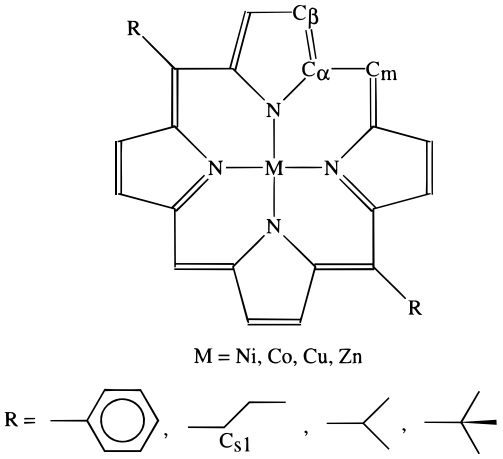

Figure 1. Molecular structures of the 5,15-disubstituted porphyrins (hydrogen atoms not shown).

Materials and Methods

Synthesis of the 5,15-Disubstituted Metalloporphyrins. The synthesis of the free bases and nickel(II) complexes of the 5,15-disubstituted porphyrins has been described in our earlier paper.[8] Cobalt(II), copper(II), and zinc(II) complexes were prepared and characterized as described below.

Co(dPP). To a solution of free base H_2dPP (40 mg) in degassed $CHCl_3$ (20 mL) was added 300 mg of $Co(Acac)_2$. The reaction mixture was refluxed for 4 h under argon and filtered through a short silica gel column, and the porphyrin was eluted with CH_2Cl_2. The solvent was then removed under vacuum, and the cobalt complex was recrystallized from CH_2Cl_2. Yield = 35 mg (78%). Mp: >300 °C. NMR: δ_H (ppm) ($C_6D_5CH_3$) 28.1 (br, 2H, H_{meso}), 16.9 and 15.4 (br, 4H each, β-H), 12.2 (br, 4H, H_{ortho}), 9.43 (br, 4H, H_{meta}), 9.26 (br, 2H, H_{para}). Anal. Calcd for $C_{32}H_{20}N_4Co$: C, 73.99; H, 3.88; N, 10.79. Found C, 73.85; H, 3.92; N, 10.77.

Cu(dPP). H_2dPP (100 mg) dissolved in $CHCl_3$/THF/MeOH (10 mL/10 mL/5 mL) was treated with $Cu(OAc)_2 \cdot H_2O$ (240 mg) and refluxed for 2 days. The reaction mixture was passed through a bed of Al_2O_3 (grade III), rinsed thoroughly with THF, and evaporated to dryness. The residue was recrystallized from CH_2Cl_2/MeOH to yield 92 mg of the title compound (yield = 81%). Mp: >300 °C. Anal. Calcd for $C_{32}H_{20}N_4Cu \cdot (H_2O)_{0.25}$: C, 72.71; H, 3.91; N, 10.60. Found: C, 72.92; H, 3.91; N, 10.68.

Zn(dPP). To a solution of H_2dPP (60 mg) in THF (20 mL) was added a saturated solution of $Zn(OAc)_2$ in MeOH (4 mL). The mixture was refluxed overnight, cooled to room temperature, and filtered through a short column of Al_2O_3 (grade III), and the porphyrin was eluted with CH_2Cl_2. The residue was recrystallized from methylene chloride to yield 60 mg (88%) of the title compound. Mp: >300 °C. NMR: δ_H (ppm) ($CDCl_3$) 10.24 (s, 2H, H_{meso}), 9.36 (d, 4H, β-H), 9.06 (d, 4H, β-H), 8.17 (m, 4H, H_{ortho}), 7.68 (m, 6H, H_{meta} and H_{para}). Anal. Calcd for $C_{32}H_{20}N_4Zn \cdot H_2O$: C, 70.60; H, 4.08; N, 10.30. Found: C, 70.60; H, 3.80; N, 10.11.

Co(dPrP) was prepared using the same procedure as described for Co(dPP) and recrystallized from CH_2Cl_2. Mp: >300 °C. Anal. Calcd for $C_{26}H_{24}N_4Co$: C, 69.48; H, 5.36; N, 12.41. Found: C, 69.21; H, 5.45; N, 12.33. Co(dPrP) was not sufficiently soluble in $CDCl_3$, CD_2Cl_2, or $C_6D_5CD_3$ to allow the measurement of a proton NMR spectrum.

Cu(dPrP) was prepared using the same procedure as described for Cu(dPP) and recrystallized from CH_2Cl_2. Mp: >300 °C. Anal. Calcd

(7) Jentzen, W.; Simpson, M. C.; Hobbs, J. D.; Song, X.-Z.; Ema, T.; Nelson, N. Y.; Medforth, C. J.; Smith, K. M.; Veyrat, M.; Mazzanti, M.; Ramasseul, R.; Marchon, J.-C.; Takeuchi, T.; Goddard, W. A., III; Shelnutt, J. A. *J. Am. Chem. Soc.* **1995**, *117*, 11085.
(8) Song, X.-Z.; Jentzen, W.; Jia, S.-L.; Jaquinod, L.; Nurco, D. J.; Medforth, C. J.; Smith, K. M.; Shelnutt, J. A. *J. Am. Chem. Soc.* **1996**, *118*, 12975.
(9) Jentzen, W.; Song, X.-Z.; Shelnutt, J. A. *J. Phys. Chem. B* **1997**, *101*, 1684.
(10) Jentzen, W.; Ma, J.-G.; Shelnutt, J. A. *Biophys. J.* **1998**, *74*, 753.
(11) (a) Sparks, L. D.; Medforth, C. J.; Park, M.-S.; Chamberlain, J. R.; Ondrias, M. R.; Senge, M. O.; Smith, K. M.; Shelnutt, J. A. *J. Am. Chem. Soc.* **1993**, *115*, 581. (b) Medforth, C. J.; Berber, M. D.; Smith, K. M.; Shelnutt, J. A. *Tetrahedron Lett.* **1990**, *31*, 3719. (c) Medforth, C. J.; Senge, M. O.; Smith, K. M.; Sparks, L. D.; Shelnutt, J. A. *J. Am. Chem. Soc.* **1992**, *114*, 9859.

for $C_{26}H_{24}N_4Cu\cdot(H_2O)_{0.25}$: C, 67.81; H, 5.36; N, 12.16. Found: C, 67.67; H, 5.03; N, 12.01.

Zn(dPrP) was prepared using the same procedure as described for Zn(dPP) and recrystallized from CH_2Cl_2/cyclohexane. Mp: >300 °C. NMR: δ_H (ppm) ($CDCl_3$ + 10 equiv of pyridine) 10.02 (s, 2H, H_{meso}), 9.64 (d, 4H, β-H), 9.37 (d, 4H, β-H), 5.08 (t, 4H, α-CH_2), 2.58 (m, 4H, β-CH_2), 1.31 (t, 6H, CH_3). Anal. Calcd for $C_{26}H_{24}N_4Zn\cdot(H_2O)_{0.5}$: C, 66.89; H, 5.40; N, 12.00. Found: C, 67.10; H, 5.23; N, 11.73.

Co(diPrP) was prepared using the same procedure as described for Co(dPP) and recrystallized from CH_2Cl_2/cyclohexane. Mp: >300 °C. NMR: δ_H (ppm) ($CDCl_3$) 27.5 (br, 2H, H_{meso}), 16.48 (br, 4H, β-H), 15.32 (br, 4H, β-H), 12.99 (br, 2H, CH), 6.26 (br, 12H, CH_3). Anal. Calcd for $C_{26}H_{24}N_4Co$: C, 69.48; H, 5.36; N, 12.41. Found: C, 69.01; H, 5.48; N, 12.34.

Cu(diPrP) was prepared using the same procedure as described for Cu(dPP) and recrystallized from CH_2Cl_2/methanol. Mp: >300 °C. Anal. Calcd for $C_{26}H_{24}N_4Cu\cdot(H_2O)_{0.5}$: C, 67.15; H, 5.42; N, 12.05. Found: C, 66.92; H, 5.12; N, 11.80.

Zn(diPrP) was prepared using the same procedure as described for Zn(dPP) and recrystallized from $CHCl_3$/cyclohexane. Mp: >300 °C. NMR: δ_H (ppm) ($CDCl_3$ + 20 equiv of pyridine) 10.03 (s, 2H, H_{meso}), 9.82 (d, 4H, β-H), 9.36 (d, 4H, β-H), 5.83 (m, 2H, CH), 2.50 (d, 12H, CH_3). Anal. Calcd for $C_{26}H_{24}N_4Zn$: C, 68.20; H, 5.28; N, 12.24. Found: C, 68.20; H, 5.60; N, 11.84.

Co(dtBuP) was prepared using the same procedure as described for Co(dPP) and recrystallized from CH_2Cl_2/methanol. Mp: >300 °C. NMR: δ_H (ppm) ($CDCl_3$) 23.6 (br, 2H, H_{meso}), 15.46 (br, 8H, β-H), 5.61 (br, 18H, CH_3). Anal. Calcd for $C_{28}H_{28}N_4NCo$: C, 70.14; H, 5.89; N, 11.68. Found: C, 69.35; H, 5.68; N, 11.43.

Cu(dtBuP) was prepared using the same procedure as described for Cu(dPP) and recrystallized from $CHCl_3$/toluene. Mp: >300 °C. Anal. Calcd for $C_{28}H_{28}N_4Cu\cdot H_2O$: C, 66.98; H, 6.02; N, 11.16. Found: C, 66.97; H, 5.68; N, 11.06.

Zn(dtBuP) was prepared using the same procedure as described for Zn(dPP) and recrystallized from $CHCl_3$/cyclohexane. Mp: >300 °C. NMR: δ_H (ppm) 9.62 (d, 4H, β-H), 9.53 (s, 2H, H_{meso}), 8.89 (d, 4H, β-H), 2.43 (s, 18H, CH_3). Anal. Calcd for $C_{28}H_{28}N_4Zn$: C, 69.21; H, 5.81; N, 11.53. Found: C, 69.06; H, 5.42; N, 11.80.

X-ray Crystallography. Crystals were transferred directly from crystallization tubes to a light hydrocarbon oil (Paratone N), in which they were examined and cut as necessary. Crystals were mounted on glass fibers and placed on a Siemens R3 m/V diffractometer equipped with graphite-monochromated Mo Kα radiation from a normal-focus sealed tube operating at 2.0 kW [Cu(dtBuP) and Zn(diPrP)(py)] or on a Syntex $P2_1$ diffractometer equipped with graphite-monochromated Cu Kα radiation from a normal-focus sealed tube operating at 2.0 kWa [Ni(diPrP)]. The crystals were cooled to 130(2) K using a stream of anhydrous nitrogen supplied from a locally modified Nonius low-temperature apparatus (Siemens R3 m/V) or a Syntex LT-1 system (Syntex $P2_1$). Data for Cu(dtBuP) were collected to $2\theta_{max} = 45.0°$ with ω scans in the index ranges $0 = h = 8$, $0 = k = 27$, $-11 = l = 11$. A total of 3253 reflections were collected including 2927 independent reflections ($R_{int} = 0.023$). Data for Zn(diPrP)(py) were collected to $2\theta_{max}$ of 55.1° with ω scans in the index ranges $0 = h = 13$, $-20 = k = 20$, $-21 = l = 21$, for a total of 11 745 independent reflections. Data for Ni(diPrP) were collected to $2\theta_{max}$ of 114.1° with $\theta/2\theta$ scans in the index ranges $0 = h = 14$, $0 = k = 20$, $0 = l = 21$, for a total of 3187 reflections and 2790 independent reflections ($R_{int} = 0.008$). Structures were solved with direct methods and refined with a full-matrix least-squares method (based on $|F^2|$ and all independent reflections) using Siemens SHELXTL version 5.03 software. Hydrogen atom positions were generated using idealized geometries and refined using riding models. Empirical absorption corrections were applied (XABS2).[12] All non-hydrogen atoms were refined with anisotropic thermal parameters. Additional experimental details are presented in Table 1.

Table 1. Data Acquisition and Structure Refinement Parameters for Cu(dtBuP), Ni(diPrP), and Zn(diPrP)(py)

	Cu(dtBuP)	Ni(diPrP)	Zn(diPrP)(py)
empirical formula	$C_{28}H_{28}N_4Cu$	$C_{26}H_{24}N_4Ni$	$C_{31}H_{29}N_5Zn$
formula wt	484.1	451.2	537.0
cryst color	purple	red	red
cryst syst	monoclinic	orthorhombic	triclinic
space group	$P2_1/n$	$Pbca$	$P\bar{1}$
a (Å)	8.026(2)	18.466(4)	10.198(3)
b (Å)	25.745(5)	12.120(2)	15.605(4)
c (Å)	10.808(2)	18.493(4)	16.815(3)
α (deg)	90	90	89.34(2)
β (deg)	92.39(3)	90	79.84(2)
γ (deg)	90	90	75.85(2)
V (Å^3)	2231.4(8)	4138.9(14)	2552.7(11)
Z	4	8	4
R1 (obs. data)	0.035	0.046	0.049
wR2 (all data)	0.084	0.122	0.126
GOF (F^2)	1.050	0.914	0.979

Molecular Modeling Studies. Classical molecular mechanics calculations have previously been used for predicting porphyrin structures by our group,[7,8,11a,13] Munro,[14] Marques,[15] and Kollman[16] et al. Molecular mechanics calculations were carried out using POLYGRAF software (Molecular Simulations, Inc.). The porphyrin force field[13a] was developed on the basis of the DREIDING II force field[17] and the normal coordinate analysis of NiOEP.[18] The unconstrained equilibrium bond length for the nickel−nitrogen(pyrrole) bond was set to 1.855 Å, and the other equilibrium bond distances and angles were adjusted so that the energy-minimized conformation of NiOEP matched the planar crystal structure of NiOEP[19] as closely as possible. This original force field has been modified as follows: (1) Parameters for additional metals were obtained by changing the equilibrium M−N bond distance R_{eq} [1.855 Å for Ni(II), 1.930 Å for Co(II), 1.970 Å for Cu(II), and 2.070 Å for Zn(II)], the homonuclear nonbond separation R_{nb} [2.27 Å for Ni(II), 3.40 Å for Co(II), 3.40 Å for Cu(II), and 4.54 Å for Zn(II)], and the atomic mass [58.700 for Ni(II), 58.933 for Co(II), 63.546 for Cu(II), and 65.380 for Zn(II)].[11a] R_{eq} of the metals is obtained by fitting planar metalloporphyrin X-ray structures.[20] (2) Electrostatic terms were included in calculating the total energy.[21] (3) The van der Waals potential energy term for hydrogen atoms was changed from a Lennard-Jones 6-12 to an exponential-6 functional form.[22] (4) A cutoff distance of 50 Å instead of 9 Å was employed when electrostatic and van der Waals energy terms were calculated.[22] (5) DREIDING II parameters

(12) Parkin, S. R.; Moezzi, B.; Hope, H. *J. Appl. Crystallogr.* **1995**, *28*, 53.

(13) (a) Shelnutt, J. A.; Medforth, C. J.; Berber, M. D.; Barkigia, K. M.; Smith, K. M. *J. Am. Chem. Soc.* **1991**, *113*, 4077. (b) Shelnutt, J. A.; Majumder, S. A.; Sparks, L. D.; Hobbs, J. D.; Medforth, C. J.; Senge, M. O.; Smith, K. M.; Miura, M.; Luo L.; Quirke, J. M. E. *J. Raman Spectrosc.* **1992**, *23*, 523. (c) Anderson, K. K.; Hobbs, J. D.; Luo, L.; Stanley, K. D.; Quirke, J. M. E.; Shelnutt, J. A. *J. Am. Chem. Soc.* **1993**, *115*, 12346. (d) Sparks, L. D.; Anderson, K. K.; Medforth, C. J.; Smith, K. M.; Shelnutt, J. A. *Inorg. Chem.* **1994**, *33*, 2297.

(14) (a) Munro, O. Q.; Marques, H. M.; Debrunner, P. G.; Mohanrao, K.; Scheidt, W. R. *J. Am. Chem. Soc.* **1995**, *117*, 935. (b) Munro, O. Q.; Bradley, J. C.; Hancock, R. D.; Marques, H. M.; Marsicana, F. *J. Am. Chem. Soc.* **1992**, *114*, 7218.

(15) (a) Marques H. M.; Munro, O. Q.; Grimmer, N. E.; Levendis, D. C.; Marsicano, F.; Pattrick, G.; Markonlides, T. *J. Chem. Soc., Faraday Trans.* **1995**, *91*, 1741. (b) Hancock, R. D.; Weaving, F. S.; Marques, H. M. *J. Chem. Soc., Chem. Commun.* **1989**, 1177.

(16) (a) Kollman, P. A.; Grootenhuis, D. D. J.; Lopez, M. A. *Pure Appl. Chem.* **1989**, *61*, 593. (b) Lopez, M. A.; Kollman, P. A. *J. Am. Chem. Soc.* **1989**, *111*, 6212.

(17) Mayo, S. L.; Olafson, B. D.; Goddard, W. A., III, *J. Phys. Chem.* **1990**, *94*, 8897.

(18) (a) Li, X.-Y.; Czernuszewics, R. S.; Kincaid, J. R.; Spiro, T. G. *J. Am. Chem. Soc.* **1989**, *111*, 7012. (b) Li, X.-Y.; Czernuszewics, R. S.; R. S.; Kincaid, J. R.; Su, Y. O.; Spiro, T. G. *J. Phys. Chem.* **1990**, *94*, 31. (c) Li, X.-Y.; Czernuszewics, R. S.; Kincaid, J. R.; Stein, P.; Spiro, T. G. *J. Phys. Chem.* **1990**, *94*, 47. (d) Kitagawa, T.; Abe; M.; Ogoshi, H. *J. Chem. Phys.* **1978**, *69*, 4516. (e) Abe, M.; Kitagawa, T.; Kyogoku, Y. *J. Chem. Phys.* **1978**, *69*, 4526.

(19) Brennan, T. D.; Scheidt, W. R.; Shelnutt, J. A. *J. Am. Chem. Soc.* **1988**, *110*, 3919.

Table 2. Selected Bond Lengths (Å) and Bond Angles (deg) and Other Structural Parameters Obtained from Crystal Structures of Metal Di-*tert*-butylporphyrins

	Ni(dtBuP)		Cu(dtBuP)		*trans*-Ni(diPrP)		*trans*-Zn(diPrP)(py)	
	10,20	5,15	10,20	5,15	10,20	5,15	10,20	5,15
				Displacements (Å)[a]				
mean	0.40[b]		0.31		0.26		0.05	
M	0.17		0.21		0.07		0.42	
N	0.12		0.16		0.05		0.06	
C_α	−0.40	0.47	−0.30	0.38	−0.28	0.32	0.04	0.00
C_β	−0.44	−0.14	−0.42	−0.03	−0.26	0.15	−0.05	−0.08
C_m	−0.70	0.89	−0.53	0.72	−0.49	0.56	0.05	−0.02
				Bond Lengths (Å)				
M−N	1.897(2)		1.973(3)		1.930(2)		2.075(2)	
N−C_α	1.380(4)	1.386(3)	1.374(4)	1.381(4)	1.383(4)	1.388(4)	1.368(4)	1.377(4)
C_α−C_β	1.429(4)	1.446(4)	1.432(5)	1.446(5)	1.428(5)	1.444(5)	1.437(5)	1.452(5)
C_α−C_m	1.381(4)	1.403(3)	1.385(5)	1.409(5)	1.372(4)	1.391(5)	1.384(5)	1.401(6)
C_β−C_β	1.352(4)		1.346(5)		1.349(5)		1.331(6)	
				Bond Angles (deg)				
N−M−N adj	92.3(1)	87.7(1)	92.7(1)	87.3(1)	91.8(1)	88.2(1)	90.7(1)	86.3(1)
N−M−N opp	177.0(1)		177.2(1)		179.2(1)		161.2(1)	
M−N−C_α	124.7(2)	128.9(2)	123.5(2)	129.2(2)	125.6(2)	129.0(2)	123.9(2)	128.5(2)
N−C_α−C_m	124.2(2)	124.2(2)	124.9(3)	124.7(3)	124.7(3)	125.6(3)	125.6(3)	125.8(3)
N−C_α−C_β	110.3(2)	108.7(2)	109.7(3)	108.3(3)	110.6(3)	109.4(3)	109.4(3)	108.0(3)
C_α−N−C_α	106.2(2)		106.9(3)		105.4(2)		107.3(3)	
C_α−C_m−C_α	123.7(3)	117.3(2)	126.3(2)	119.1(3)	124.6(3)	119.6(3)	128.2(3)	126.3(3)
C_α−C_α−C_β	107.3(2)	107.9(3)	107.1(3)	108.0(3)	107.1(3)	107.5(3)	107.4(3)	108.0(3)
C_m−C_α−C_β	125.3(3)	126.4(3)	125.4(3)	126.5(3)	124.5(3)	124.7(3)	125.0(3)	126.2(3)

[a] From the least-squares plane of the 24 atoms of the porphyrin core. [b] A single value indicates only one displacement, bond length, or bond angle for the molecule.

were used consistently instead of a hybrid of DREIDING I for the macrocycle and DREIDING II for the substituents.[7] (6) Torsions for resonance atom types exocyclic to aromatic ring systems were reduced to 40% of the value internal to the ring, consistent with DREIDING II.[17] (7) A minor error in the counting of the nonbond interactions of the atoms bonded to the metal was corrected in the POLYGRAF code.[8] (8) The *r*-dependent dielectric constant of 2.64 for CS_2 was used instead of 1.00 for vacuum in the calculations of electrostatic energy terms, mimicking the experimental solvent environment.[8] These modifications have only a minor influence on the calculated porphyrin structures but affect the relative energies of conformers. After these changes, the force field bond distances and angles for the macrocycle were reoptimized using a least-squares method.[23]

The most important change in the force field is a reduction in the out-of-plane force constants by 50%,[8] which approximately corrects for the addition of the out-of-plane and in-plane force constants independently obtained from separate normal coordinate analyses. This revision improves the ability of the force field to predict the structures of nonplanar porphyrins and gives more accurate relative energies of the stable porphyrin conformers.

Resonance Raman Spectroscopy. Resonance Raman spectra were obtained using a partitioned Raman cell and a dual-channel spectrometer described previously.[24] Approximately 0.1 mM CS_2 solutions of the sample and a reference porphyrin [nickel(II) tetraphenylporphyrin (NiTPP)] were placed in a dual-compartment cell. The 413.1-nm line from a krypton ion laser (Coherent, INNOVA 20) was used for excitation in the B band region. The scattered light was collected in the 90° scattering geometry, and the Raman cell was rotated at 50 Hz to prevent local heating of the sample and to alternately probe the sample and reference solutions. Typical conditions for the spectra of the nickel(II), cobalt(II), and copper(II) porphyrins were 50−60-mW laser power, approximately 2.7-cm^{-1} spectral slit width, 4−6 scans with 0.3-cm^{-1} step increment, and 1-s integration time. Since the zinc(II) porphyrins decomposed during the measurements, lower laser power (20 mW), fewer scans (2−3), larger step increments (0.5), and shorter integration times (0.5 s) were used. The frequencies in the regions above and below 900 cm^{-1} were calibrated with the 1373.3- (ν_4) and 391.9-cm^{-1} (ν_8) lines of NiTPP.[25] In addition, all the spectra were corrected for the nonlinearity of the spectrometer to obtain the absolute frequencies of the lines to an accuracy of ± 1 cm^{-1}.[25]

Results

Crystal Structures of Metal Complexes of the 5,15-Dialkylporphyrins. In an earlier study, we reported preliminary data from the crystal structures of Ni(dPP), Ni(dPrP), and Ni(diPrP) and full details of the crystal structure of Ni(dtBuP).[8] To investigate the metal dependence of the nonplanar distortions of the 5,15-dialkylporphyrins in this work, X-ray crystal structures were determined for complexes with other metals, namely, the copper(II) complex of dtBuP (Cu(dtBuP)) and the monopyridine zinc(II) complex of diPrP [Zn(diPrP)(py)]. Full details of the crystal structure of Ni(diPrP) are presented elsewhere.[25] Table 1 gives details of the data acquisition and structure refinement parameters for Cu(dtBuP), Ni(diPrP), and Zn(diPrP)(py). Out-of-plane displacements, bond lengths, and bond angles for Ni(dtBuP), Cu(dtBuP), Ni(diPrP), and Zn(diPrP)(py) are summarized in Table 2. Note for the diPrP complex that either the methyl groups of both isopropyl groups can point toward C10 or C20 (cis conformation) or the methyl groups of one isopropyl can point toward C10 and the methyls

(20) (a) Dewyer, P. N.; Madura, P.; Scheidt, W. R. *J. Am. Chem. Soc.* **1974**, *96*, 4815. (b) Pak, R.; Scheidt, W. R. *Acta Crystallogr.* **1991**, *c47*, 431. (c) Collins, D. M.; Hoard, J. L. *J. Am. Chem. Soc.* **1970**, *92*, 3761. (d) Scheidt, W. R.; Cunningham, J. A.; Hoard, J. L. *J. Am. Chem. Soc.* **1973**, *95*, 8289. (e) Reed, C. A.; Mashiko, T.; Bentley, S. P.; Kastner, M. E.; Scheidt, W. R.; Spartalian, K.; Lang, G. *J. Am. Chem. Soc.* **1979**, *101*, 581.
(21) Sparks, L. D.; Chamberlain, J. R.; Hsu, P.; Ondrias, M. R.; Swanson, B. A.; Oritiz de Montellano, P. R.; Shelnutt, J. A. *Inorg. Chem.* **1993**, *32*, 3153.
(22) Hobbs, J. D.; Majumder, S. A.; Luo, L.; Sickelsmith, G. A.; Quirke, J. M. E.; Medforth, C. J.; Smith, K. M.; Shelnutt, J. A. *J. Am. Chem. Soc.* **1994**, *116*, 3261.
(23) Dasgupta, S.; Goddard, W. A., III. *J. Chem. Phys.* **1989**, *90*, 207.
(24) Shelnutt, J. A. *J. Phys. Chem.* **1983**, *87*, 605.
(25) Jentzen, W.; Turowska-Tyrk, I.; Scheidt, W. R.; Shelnutt, J. A. *Inorg. Chem.* **1996**, *35*, 3559.
(26) Nurco, D. J.; Medforth, C. J.; Smith, K. M. Unpublished results.

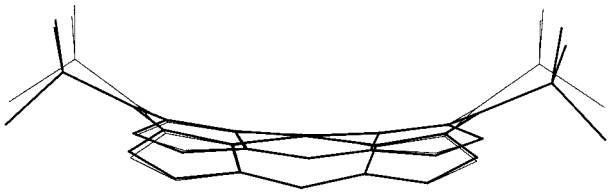

Figure 2. Comparison of the X-ray crystal structure (heavy) and the energy-optimized structure (light) for copper(II) di-*tert*-butylporphyrin.

of the other isopropyl toward C20 (trans conformation). The crystal structure of Ni(diPrP) shows a trans conformation, whereas both cis and trans conformers are observed in the unit cell of Zn(diPrP)(py). For consistency, the data given for Zn(diPrP)(py) in Table 2 is for the trans conformer only. Complete information on the crystal structures is given in the Supporting Information.

The crystal structure of Cu(dtBuP) is shown in Figure 2 and is generally similar to that previously reported for NidtBuP.[8] The differences between the two structures can be related to the smaller metal atom in NidtBuP, which favors shorter metal−nitrogen bond distances and a more nonplanar macrocycle.[7,8] For example, the average M−N distance seen for Ni(dtBuP) [1.897(2) Å] is significantly shorter than that seen for Cu(dtBuP) [1.973(3) Å], and the mean out-of-plane displacement (0.40 Å) is greater than that observed for Cu(dtBuP) (0.31 Å). Similar metal effects are seen for *trans*-Ni(diPrP) and *trans*-Zn(diPrP)(py), where the Zn−N distance is 2.075(2) Å and the Ni−N distance 1.930(2) Å, and the mean out-of-plane displacements are 0.05 and 0.26 Å, respectively.

The bond lengths and bond angles for the diPrP and dtBuP complexes (Table 2) provide insights into the structural deformations of these porphyrins. Significant differences are observed between the bond lengths and bond angles associated with the 5,15 axis (bearing the substituents) and those associated with the 10,20 axis (unsubstituted). The largest differences are seen for the $N-M-N_{adj}$, $M-N-C_\alpha$, and $C_\alpha-C_m-C_\alpha$ bond angles (Table 2). Similar differences have recently been seen in 2,3,5,7,8,12,13,15,17,18-decasubstituted porphyrins[26,27] and were attributed to the need to minimize steric strain between the 5,15 meso-substituents and the alkyl groups at the pyrrole positions. It is likely that a related steric interaction, in this case between the meso substituents and the pyrrole rings, is present in the 5,15-dialkylporphyrins. Other differences in the bond angles and bond lengths associated with the 5,15 and 10,20 axes are smaller. For example, the 5,15 $N-C_\alpha$, $C_\alpha-C_m$, and $C_\alpha-C_\beta$ bond lengths are longer than those for the 10,20 axis. Likewise, the $N-C_\alpha-C_\beta$ bond angles are smaller and the $C_\alpha-C_\beta-C_\beta$ and $C_m-C_\alpha-C_\beta$ bond angles are larger along the 5,15 axis. Typically, these structural differences are also observed in the energy-optimized structures of these porphyrins.

Calculation of Minimum-Energy Structures for the Metal Complexes of the 5,15-Dialkylporphyrins. Molecular mechanics calculations generally predict that the 5,15-disubstituted metalloporphyrins have two types of primary conformations resulting from different orientations of the first meso-bonded carbon (C_{s1}) of the 5 and 15 substituents relative to the porphyrin macrocycle. The most stable conformer has the αα configuration, with the C_{s1} atoms of the two substituents on the same side of the macrocycle. The higher-energy αβ conformer has the C_{s1} atoms of the two substituents on opposite sides of the macrocycle. When the C_{s1} of the substituent is asymmetrically substituted (like propyl and isopropyl), there are secondary conformers resulting from the different possible orientations of C_{s2} (the second substituent carbon from the ring). These secondary substituent configurations are labeled "cis" when the C_{s2} atoms are on the same side of the vertical plane through the 5 and 15 positions and "trans" when the C_{s2} atoms are on opposite sides of this plane.[8] Table 3 summarizes the structural parameters calculated for the most stable planar and αα conformers for each 5,15-disubstituted metalloporphyrin. The structural parameters for the higher-energy αβ conformers are given in Table S1 of the Supporting Information. The calculated energies for all of the stable conformations of the 5,15-disubstituted metalloporphyrin are given in Table S2 of the Supporting Information.

A planar conformer is predicted for each metal complex of dPP; the only stable nonplanar conformation is the αα conformer of Ni(dPP). The energies of the planar and αα conformers of Ni(dPP) are almost the same. There is no αβ conformer predicted for the diphenylporphyrins regardless of the metal in the macrocycle.

For dPrP, six stable conformers (αα, *trans*-αα, *cis*-αα, αβ, *trans*-αβ, and *cis*-αβ) are predicted for each metalloporphyrin. The αα conformer is the most stable one. The conformational energy difference ($\Delta E = E_{\alpha\beta} - E_{\alpha\alpha}$) decreases as the metal size increases (Ni < Co < Cu < Zn), and the differences are all within 3 kcal/mol. Because of the latter, it is possible that many of these conformers coexist in solution. Only the structural parameters and energies of representative αα and αβ conformers are tabulated in Table 3 and Tables S1 and S2 of the Supporting Information.

For diPrP, each metalloporphyrin has four stable conformers (*trans*-αα, *cis*-αα, *trans*-αβ, and *cis*-αβ). The averaged structural parameters of the αα or the αβ conformers are almost the same, so only the structural parameters of the trans conformers are given in Table 3 and Tables S1 and S2. Δ*E* again decreases as the metal size increases. For Ni(diPrP), Δ*E* is large (4.59 kcal/mol), so only the αα conformers exist in solution. Δ*E* decreases dramatically with the increasing size of the central metal and falls to within 3 kcal/mol for Co(diPrP), Cu(diPrP), and Zn(diPrP), indicating that all four conformers may coexist in solution for these metals.

For dtBuP, the symmetry of the *tert*-butyl substituent allows only αα and αβ conformers. Δ*E* between these two conformers is large (over 6 kcal/mol) for every porphyrin, although here too Δ*E* decreases as the metal size increases. The large Δ*E* means that only the αα conformer is present in solution.

Modeling the Metal Dependence of Symmetric Deformations. The out-of-plane distortions seen for the 5,15-disubstituted porphyrins are mixtures of symmetric distortions, mainly ruffling and doming of the macrocycle. To understand the metal dependence of these basic symmetric deformations, a series of macrocyclic structures with different degrees of nonplanar distortion and different symmetric deformation types were generated from *meso*-tetra-(*tert*-butylporphyrin (TtBuP, without methyl hydrogens) by orienting the substituents. Specifically, the *dom* structure was given by the αααα orientation (all four substituents above the macrocycle plane), the *ruf* structure was given by the αβαβ orientation (substituents alternatively above and below the porphyrin plane), and the *wav* structure was given by the ααββ orientation. The pure *sad* structures were obtained from *meso*-tetraphenylporphyrin (TPP) instead of TtBuP, which does not form a saddled structure. The purity of the distortion

(27) (a) Medforth, C. J.; Senge, M. O.; Forsyth, T. P.; Hobbs, J. D.; Shelnutt, J. A.; Smith K. M. *Inorg. Chem.* **1994**, *33*, 3865. (b) Senge, M. O.; Medforth, C. J.; Forsyth, T. P.; Lee, D. A.; Olmstead, M. M.; Jentzen, W.; Pandey, R. K.; Shelnutt, J. A.; Smith K. M. *Inorg. Chem.*, in press.

Table 3. Selected Structural Parameters Obtained from the Most Stable Calculated Conformations of the Metal 5,15-Disubstituted Porphyrins

porphyrin	Ni−N% (Å)	dihed angle (deg)	$C_\alpha-N-C_\alpha$ (deg)	N−Ni−N (deg)	$C_\beta-C_\beta$ (Å)	$C_\alpha-C_m$ (Å)	$C_\alpha-N$ (Å)	$NC_\alpha-C_\beta C_\beta$ (deg)	$NC_\alpha-C_mC_\alpha$ (deg)
planar dPP									
Ni	1.949	0.2	104.3	180.0	1.326	1.378	1.382	0.0	0.0
Co	1.979	0.0	105.3	180.0	1.329	1.383	1.380	0.0	0.0
Cu	1.995	0.1	105.9	180.0	1.331	1.386	1.378	0.0	0.0
Zn	2.036	0.1	107.3	180.0	1.335	1.394	1.376	0.0	0.0
αα-dPP									
Ni	1.944	12.7	104.4	179.8	1.326	1.378	1.382	0.8	4.9
αα-dPrP									
Ni	1.929	24.7	104.9	179.2	1.328	1.381	1.381	1.2	10.1
Co	1.970	15.4	105.6	179.1	1.329	1.385	1.380	0.6	7.2
Cu	1.990	11.6	106.0	179.0	1.331	1.388	1.379	0.4	5.8
Zn	2.033	6.2	107.3	178.7	1.334	1.395	1.376	0.3	3.8
trans-αα-diPrP									
Ni	1.913	33.2	105.4	178.2	1.330	1.384	1.379	1.1	14.8
Co	1.956	26.0	106.0	177.7	1.331	1.387	1.378	1.0	13.0
Cu	1.978	22.5	106.4	177.4	1.332	1.390	1.377	1.4	12.0
Zn	2.028	14.8	107.6	176.0	1.335	1.402	1.377	0.8	9.5
αα-dtBuP									
Ni	1.892	41.4	106.0	175.9	1.334	1.387	1.376	2.0	20.5
Co	1.935	35.7	106.6	174.6	1.335	1.390	1.375	1.9	19.6
Cu	1.958	32.9	107.0	173.7	1.336	1.392	1.374	1.8	19.2
Zn	2.018	26.3	107.9	168.9	1.338	1.398	1.374	1.3	17.8

in each structure was checked by decomposing the structure into symmetric components (*ruf*, *sad*, *dom*, *wav*, see below). The degree of the distortion for each of the structures was altered by changing the van der Waals distance parameter of the substituent carbons (from 0.5 to 5 Å in increments of 0.5 Å). The calculations were carried out for each of the metals. Figure 3 shows the plots of the resulting metal−nitrogen (M−N) distance as a function of total deformation (obtained from normal-coordinate structural decomposition) for the *ruf*, *dom*, and *wav* types of deformation.

Structural Decomposition of the X-ray Crystal Structures and Calculated Structures. The available X-ray structures and the calculated stable conformers for the series of 5,15-disubstituted porphyrins were structurally decomposed in terms of displacements along the lowest-frequency out-of-plane normal coordinates of the macrocycle by using the normal-coordinate structural decomposition (NSD) method. NSD results are given for both *minimal* and *extended* basis sets of normal-coordinate eigenvectors (see Discussion).[9] Table 4 tabulates the decomposition results obtained using the minimal basis set for the X-ray structures and the most stable calculated conformations. The results obtained using the extended basis for these conformations are shown in Table S3 of the Supporting Information. The decomposition results for the $\alpha\beta$ conformers obtained using the minimal and extended basis are given in Tables S4 and S5 of the Supporting Information, respectively.

Resonance Raman Spectroscopy. The 413.1-nm excited resonance Raman spectra of dPP, dPrP, diPrP, and dtBuP with Ni, Co, Cu, and Zn as central metals in high-frequency (1300−1700 cm^{-1}), low-frequency (200−600 cm^{-1}), and mid-frequency (900−1300 cm^{-1}) regions are shown in Figures S1−3 of the Supporting Information. The quality of the spectra of the zinc porphyrins is generally poor because of their strong fluorescence and partial decomposition during measurements. The frequencies of some strong Raman lines, ν_2, ν_4, ν_9, ν_6, and ν_8, are tabulated in Table 5.

The high-frequency region contains most of the structure-sensitive and oxidation-state marker lines. For porphyrins with the same central metal but different substituents, the structure-sensitive line ν_2 downshifts with the increasing steric size of the substituents. On the other hand, the oxidation-state marker line ν_4 varies little with the different substituents.

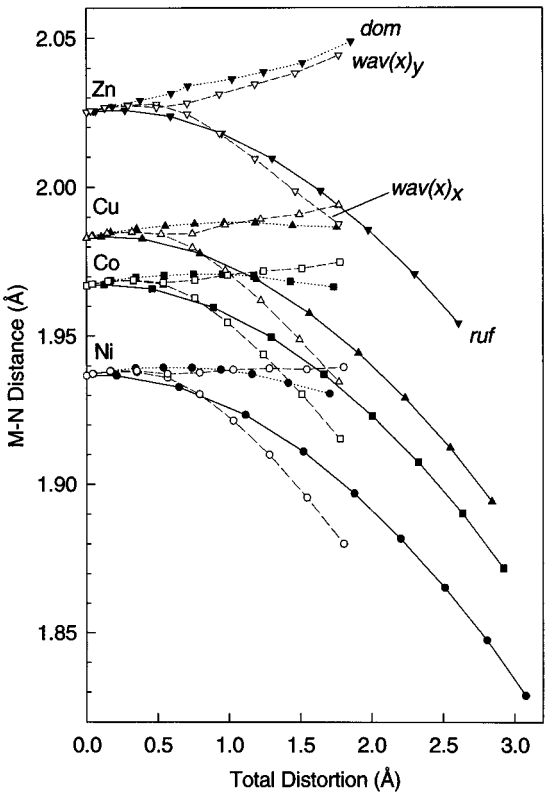

Figure 3. Metal−nitrogen distance as a function of total out-of-plane displacements of the macrocyclic atoms for pure symmetric distortions (*ruf*, *dom*, and *wav*). The curves are obtained from molecular mechanics calculations on tetra-*tert*-butyl metalloporphyrin (without hydrogen) by increasing the van der Waals radius of the substituent carbon atoms from 0.0 at 0.5-Å intervals. The deformation type is determined by the initial orientation of the substituent groups (*ruf*; $\alpha\beta\alpha\beta$; *dom*, αααα; *wav*; $\alpha\alpha\beta\beta$).

For the same porphyrin with different metals, both ν_2 and ν_4 downshift with increasing metal size. This relationship is analogous to the core-size correlation of nearly planar porphyrins.[28] A subtler trend in the variation of the Raman frequencies with metal size can also be seen. For ν_2, the range of downshifts for the metal derivatives decreases, as the porphyrin substituents become more bulky. The trend is less definite for ν_4.

Table 4. Displacements (in Å) along the Lowest-Frequency Out-of-Plane Normal Coordinates of the Macrocycle: Normal-Coordinate Structural Decomposition Results Using the Minimal Basis for the Selected Most Stable Conformers of the Series of 5,15-Disubstituted Porphyrins and the X-ray Crystal Structures (Bold)

porphyrin conformer	*ruf* B_{1u}	*sad* B_{2u}	*dom* A_{2u}	*wav*(*x*) E_{gx}	*wav*(*y*) E_{gy}	*pro* A_{1u}	d_{tot} sim	d_{tot} calcd
planar dPP								
Ni	0	0	0	0	0	0	0	0
Co	0	0	0	0	0	0	0	0
Cu	−0.005	0	0	0	0	0	0.005	0.005
Zn	−0.004	0	0	0	0	0	0.004	0.004
Ni αα	0.609	0	0.015	0	0	0	0.610	0.611
X-ray	**0.736**	**−0.075**	**0.059**	**−0.004**	**−0.048**	**0.007**	**0.744**	**0.745**
αα-dPrP								
Ni	1.186	0	0.083	0	0	0	1.189	1.193
Co	0.757	0	0.100	0	0	0	0.764	0.769
Cu	0.576	0	0.105	0	0	0	0.585	0.591
Zn	0.319	0	0.114	0	0	0	0.338	0.346
trans-αα-diPrP								
Ni	1.603	0.052	0.227	0	0	0	1.620	1.631
X-ray	**1.467**	**−0.138**	**0.202**	**0.011**	**−0.010**	**0.022**	**1.488**	**1.490**
Co	1.280	0.047	0.256	0	0	0	1.307	1.322
Cu	1.120	0.046	0.271	0	0	0	1.153	1.170
Zn	0.763	0.040	0.315	0	0	0	0.827	0.848
Zn(py)								
trans	0.860	0.032	0.347	0	0	0	0.928	0.944
cis	0.852	0	0.175	−0.012	0.012	0	0.870	0.888
X-ray trans	**0.097**	**−0.097**	**−0.259**	**0.062**	**0.053**	**−0.013**	**0.305**	**0.307**
X-ray cis	**0.523**	**−0.116**	**−0.217**	**0.024**	**−0.072**	**0**	**0.583**	**0.585**
αα-dtBuP								
Ni	2.013	0	0.541	0	0	0	2.085	2.114
X-ray	**2.181**	**−0.021**	**0.488**	**−0.079**	**0.078**	**0.007**	**2.239**	**2.249**
Co	1.773	0	0.607	0	0	0	1.874	1.909
Cu	1.656	0	0.646	0	0	0	1.778	1.816
X-ray	**1.694**	**−0.008**	**0.637**	**0.055**	**−0.005**	**−0.009**	**1.811**	**1.826**
Zn	1.368	0	0.792	0	0	0	1.581	1.625

Table 5. Frequencies of Selected Resonance Raman Lines for Metal Disubstituted Porphyrins in CS_2 Solution

porphyrin	ν_2	ν_4	ν_9	ν_6	ν_8
dPP					
Ni	1573.9	1374.4	1072.9	1001.8	397.5
Co	1567.3	1370.9	1071.8	1001.0	394.6
Cu	1560.8	1368.3	1071.0	1001.8	394.6
Zn	1547.6	1365.6	1070.3	1003.0	396.8
dPrP					
Ni	1573.3	1373.0	1076.6	1011.8	382.5
Co	1568.5	1369.9	1076.0	1007.3	377.3
Cu	1562.6	1368.2	1075.4	1009.9	378.1
Zn	1547.6	1364.9	1075.4	1010.2	378.6
diPrP					
Ni	1563.4	1374.7	1077.6	1013.9	386.1
Co	1561.1	1372.3	1077.5	1008.2	376.6
Cu	1558.3	1371.7	1079.3	1008.3	371.1
Zn	1546.0	1366.5		1008.0	369.1
dtBuP					
Ni	1548.2	1371.2	1079.0	1022.5	398.1
Co	1546.0	1367.4	1077.9	1016.8	391.6
Cu	1542.6	1365.0	1077.9	1014.4	384.5
Zn	1539.0	1355.0	1077.8	1008.1	378.9

The band shape of the strong structure-sensitive line ν_2 also exhibits systematic changes with the size of the central metal. For dPP, ν_2 of the Ni(II) compound is broad and asymmetric with an asymmetric tail on the low-frequency side; ν_2 of the Co(II) derivative is less broad and less asymmetric; the ν_2 lines of the Cu(II) and Zn(II) compounds are narrow and symmetric. For dPrP, every metalloporphyrin has a broad and asymmetric ν_2 band. For diPrP, ν_2 is almost symmetric for Ni(diPrP), but asymmetric for Co(diPrP) and Cu(diPrP) [and possibly for Zn(diPrP)]. For dtBuP, ν_2 of Ni(dtBuP) is apparently a doublet with two almost equally intense sublines; the intensity of the high-frequency subline gradually decreases in the order Ni > Co > Cu > Zn.

The Raman lines such as ν_9, ν_6, and ν_8 in the middle- and low-frequency regions show no obvious trends of the dependence of frequency on the size of the central metal and bulkiness of the substituents. However, the shape of ν_8, which is sensitive to structural heterogeneity, does show dependence on these factors. For dPP, ν_8 is broad and asymmetric for nickel and becomes less broad and asymmetric with larger cobalt, and narrow and symmetric with even larger copper. For dPrP, ν_8 is uniformly broad and asymmetric. For diPrP, the somewhat broad ν_8 line is symmetric with nickel, but asymmetric with larger metals. For dtBuP, ν_8 is narrow and symmetric with all metals.

Discussion

Representation of Metalloporphyrin Nonplanar Distortions in Terms of Displacements along the Lowest-Frequency Normal Coordinates. The nonplanar distortions of metalloporphyrins can be classified according to irreducible representations of the nominal D_{4h} point group of a square-planar porphyrin macrocycle.[7] The commonly observed *ruf* and *sad* distortions resemble the lowest-frequency normal coordinates of B_{1u} and B_{2u} symmetry, respectively, and the *dom* and occasionally observed *wav* distortions are similar to the lowest-frequency normal coordinates of A_{2u} and E_g symmetries. This suggests that a convenient way to describe these structures is in terms of the displacements along these lowest-frequency normal coordinates.

(28) (a) Parthasarathi, N.; Hanson, C.; Yamayuchi, S.; Spiro, T. G. *J. Am. Chem. Soc.* **1987**, *109*, 3865. (b) Strong, J. D.; Kubaska, R. J.; Shupack, S. I.; Spiro, T. G. *J. Raman Spectrosc.* **1980**, *9*, 312. (c) Ghottard, G.; Baccioni, P.; Baccioni, J. P.; Lange, M.; Mansuy, D. *Inorg. Chem.* **1981**, *20*, 1718.

For symmetrically substituted porphyrins with four identical meso substituents, nonplanar distortion usually occurs along only one of the lowest-frequency normal coordinates given a particular configuration of the substituents. For an asymmetrically substituted porphyrin or a porphyrin in an asymmetrical environment as in a protein, the macrocycle tends to deform along two or more of these normal coordinates.[8] In this case, the nonplanar distortion can be represented in terms of displacements along a linear combination of these normal coordinates. For a given structure, the displacements that best simulate the distortion of the macrocycle can be determined using a recently devised computational procedure, called normal-coordinate structural decomposition.[9]

Theoretically, the complete set of normal coordinates for the macrocycle forms a basis for describing any distortion of a porphyrin macrocycle. For a macrocycle with D_{4h} symmetry, the distortions can be divided into in-plane and out-of-plane deformations. Thus, any out-of-plane distortion of the macrocycle can be quantitatively represented by a linear combination of the 21 ($N - 3$) unit vectors of the out-of-plane normal coordinates (normal deformations). However, usually only a few of the lowest-frequency modes are required to adequately describe the distortion,[9] since these are the softest modes of deformation of the porphyrin. That is, the restoring forces are the smallest for displacements along the lowest-frequency normal coordinates, so displacements along the coordinates require little energy. Since the lowest-frequency B_{2u} and B_{1u} modes usually appear at lower frequency than the lowest-frequency A_{2u} mode, the *sad* and *ruf* distortions are observed more frequently than *dom* distortion. The lowest-frequency E_g mode is found at even higher frequency than the lowest-frequency A_{2u} mode, and so, the *wav* distortion is seen only occasionally. The lowest-frequency mode of A_{1u} symmetry (*pro*, propellering of the pyrroles) is so high in frequency that the *pro* deformation is rarely observed. (The calculated frequencies of the modes forming the *minimal* basis set in the NSD procedure are 88 cm^{-1} for $B_{1u}^{(1)}$, 65 cm^{-1} for $B_{2u}^{(1)}$, 335 cm^{-1} for $A_{1u}^{(1)}$, 135 cm^{-1} for $A_{2u}^{(1)}$, and 176 cm^{-1} for $E_g^{(1)}$ symmetries,[9] where the superscript (1) indicates the lowest-frequency mode of the indicated symmetry.)

To describe the out-of-plane distortions more accurately, the basis set needs to be *extended* to include the second-lowest-frequency normal mode of each symmetry type. This is especially important for the description of *dom* and *wav* distortions where the second-lowest-frequency modes for the A_{2u} and E_g symmetries are close in energy to the lowest-frequency modes. The calculated frequencies of the second-lowest-frequency modes[9] are 516 cm^{-1} for $B_{1u}^{(2)}$ ($5.9B_{1u}^{(1)}$), 721 cm^{-1} for $B_{2u}^{(2)}$ ($11.1B_{2u}^{(1)}$), 680 cm^{-1} for $A_{1u}^{(2)}$ ($2.0A_{1u}^{(1)}$), 359 cm^{-1} for $A_{2u}^{(2)}$ ($2.7A_{2u}^{(1)}$) and 238 cm^{-1} for $E_g^{(2)}$ ($1.4E_g^{(1)}$). Obviously, to obtain an exact description of the nonplanar distortion it would be necessary to include all 21 of the out-of-plane normal modes in the basis set. However, usually this is unnecessary because the displacements along the high-frequency modes are smaller than the experimental error in the X-ray crystal structures.

For the series of 5,15-disubstituted metalloporphyrins, molecular mechanics calculations predict that there are stable $\alpha\alpha$ and $\alpha\beta$ conformers as shown in Tables 3 and S1. Structural decomposition of these conformers (Tables 4 and S3−5) verifies that the distortions of this series of porphyrins occur primarily along the lowest-frequency normal coordinates for all the metals. This is clearly shown in Figures 4, S4, and S5. Figures 4, S4, and S5 show the comparisons of the simulated and experimental

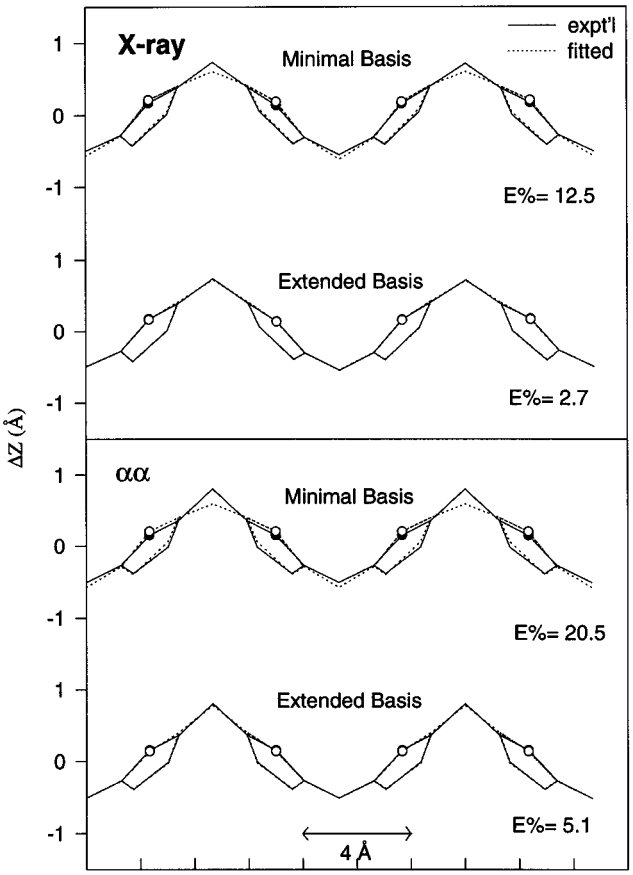

Figure 4. Comparisons of the structures simulated using the *minimal* and *extended* basis with the X-ray crystal structures and calculated trans-$\alpha\alpha$ conformers of copper di-*tert*-butylporphyrin.

out-of-plane displacements for the X-ray crystal structures of Cu(dtBuP), Ni(diPrP), and Zn(diPrP)(py) obtained using the *minimal* and *extended* basis sets. Clearly, the lowest-frequency normal deformations (minimal basis) alone adequately simulate the nonplanar distortions. Of course, the accuracy of the simulated structures improves when the extended basis set is used (Figure 4).

For the *gab* conformer, the out-of-plane displacements of the macrocyclic atoms are represented by a linear combination of the unit vectors for the lowest-frequency B_{1u} and A_{2u} coordinates. For the minimal basis set, the deviations are mainly due to the doming components, for which the contribution from the second-lowest-frequency normal mode is usually 40−80% of that of the lowest-frequency mode (Table S3 of the Supporting Information). Second-order ruffling contributions are usually only 4−14% of the lowest-frequency mode contributions, reflecting a larger frequency separation between the second-lowest- and lowest-frequency B_{1u} modes.

The same reasoning explains why the extended basis set is needed to accurately describe the $\alpha\beta$ conformers. In fact, to accurately describe the distortions of the $\alpha\beta$ conformers the basis set needs to be extended to the third-order normal modes. The $\alpha\beta$ conformer is composed of equal amounts of the *wav*(x) and *wav*(y) E_g deformations only. That higher order normal coordinates are needed for E_g distortion is not surprising given that the frequency of the third-lowest-frequency E_g mode (calculated at 467 cm^{-1} for the Cu porphyrin macrocycle) is lower than most of the second-lowest-frequency normal modes for the other symmetries.[9]

The structural decomposition results also show that the relative contributions of different normal coordinates to the total

distortion are metal dependent. To understand this result, the metal dependence of the core size was studied for each normal coordinate (Figure 3).

Dependence of the Metal−Nitrogen Distance on the Magnitude of the Deformations. The *ruf*, *dom*, and *wav* deformations have different influences on the core size (M−N distance). Conversely, incorporation of metals of different size in the center of the macrocycle will influence the relative contributions of the nonplanar deformations to the total distortion. The calculated dependence of the M−N distance on the displacement along the *ruf*, *dom*, and *wav*(*x*) normal deformations is shown in Figure 3. The *ruf* deformation reduces the average M−N distance, and thus the core-size, the most for a given amount of distortion and peripheral steric strain (see caption). The average M−N distance is used because the *wav* deformation causes a significant decrease of the M−N distance along one direction, but the M−N distance perpendicular to that direction changes little. The *sad* deformation (not shown) also reduces the core size but to a lesser degree than ruffling. The *dom* deformation does not change the M−N distance appreciably. The observations hold regardless of the metal. When the equilibrium M−N distance is larger than the optimum core size of the macrocycle (e.g., Zn), doming even causes the M−N distance to increase.

On the basis of these observations, a small metal such as nickel(II) favors ruffling the most and saddling less and disfavors doming the most and waving less; a large metal favors doming the most and disfavors ruffling the most.

Nonplanar Distortions of Metal Complexes of the 5,15-Disubstituted Metalloporphyrins. The results of normal-coordinate structural decomposition show that the gabled αα conformers consist mainly of B_{1u} *ruf* and A_{2u} *dom* symmetric deformations (Table 4 and Table S3 of the Supporting Information). The αβ conformers are a mixture of *wav*(*x*) and *wav*(*y*) deformations (Tables S4 and S5 of the Supporting Information). These structural findings can be understood qualitatively in terms of symmetry, with the aid of a correlation table for the D_{4h} group. The αα conformer has C_{2v} (C_2, σ_d) symmetry. Among the five out-of-plane symmetries in the D_{4h} point group, the A_{2u} and B_{1u} representations are totally symmetric (transform like A_1) in the C_{2v} group. Consequently, the A_{2u} and B_{1u} symmetries may mix in the lower symmetry in any combination. Similarly, the αβ conformer has C_{2h} (C''_2) symmetry, and only the E_g representations are totally symmetric (transform like A_g) in the C_{2h} group. In this case, the E_{gx} and E_{gy} deformations must mix in equal proportions.

Additional symmetries may contribute when the symmetry is further lowered by, for example, the different relative orientations of asymmetric meso substituents. In particular, because of the asymmetry of the isopropyl groups, the molecular symmetry of the trans-αα conformer of diPrP is lowered from the C_{2v} group to the C_2 (C_2) group. Moreover, in the C_2 group, in addition to the A_{2u} and B_{1u}, the B_{2u} and A_{1u} symmetries are also totally symmetric (transform like A). Thus, the *sad* and *pro* distortions are allowed to mix with *ruf* and *dom* in the lower symmetry. This then explains the small *sad* contributions in addition to the main *ruf* and *dom* contributions for the distortions of *trans*-αα-diPrPs as shown in Table 4. The distortion along the A_{1u} coordinate is zero because the perturbation energy is too small to produce a measurable distortion of this symmetry type.

Relative Contributions of Symmetric Distortions for the 5,15-Disubstituted Metalloporphyrins. In the previously studied meso-tetrasubstituted porphyrins,[7] the *ruf* and *dom* conformations result from the perturbations caused by the different orientations of the substituents. Specifically, αβαβ orientation (B_{1u} symmetry) leads to the *ruf* conformation, and the αααα orientation (A_{2u} symmetry) results in the *dom* conformation. Because these symmetries do not belong to the same representation in the lower-symmetry point groups of the molecule, the *ruf* and *dom* distortions cannot mix as they do for the αα 5,15-disubstituted porphyrins.

Since both the *ruf* and *dom* deformations can occur in any proportion in the αα conformer and since these deformations are affected by metal size differently, one might expect the relative amounts of these deformations to be influenced by metal size. For the αα conformers of the 5,15-disubstituted porphyrins, the distortion decreases dramatically along the *ruf* deformation and increases along the A_{2u} *dom* deformation, as the size of the metal atom increases (Ni < Co < Cu < Zn). This metal dependence occurs because the *ruf* deformation reduces the core size (and M−N distance), while the *dom* deformation hardly changes the M−N distance. Accordingly, when the central metal is small like Ni(II), the porphyrin macrocycle prefers a significantly shorter metal−nitrogen distance [1.85 Å for Ni(II)] than the optimum distance of about 2.00 Å for a planar porphyrin. The most efficient way to shorten the M−N distance is to ruffle the porphyrin macrocycle (Figure 3). However, this preference for ruffling decreases as the metal size increases [Co(II) and Cu(II)]. When the metal is so large that it prefers a metal−nitrogen distance larger than the optimum distance of a planar macrocycle, for example, Zn(II) (2.07 Å), ruffling is disfavored and doming is favored. Therefore, for the same 5,15-disubstituted porphyrin, the *ruf* contribution decreases as the metal changes from Ni(II) to Co(II), Cu(II), and Zn(II). As the *ruf* distortion decreases, the distortion along the A_{2u} *dom* normal coordinate increases slightly to help relieve the steric strain of the substituents. The large decrease in the *ruf* deformation with increasing metal size also results in an overall decrease in the total distortion for a given porphyrin (dPrP, diPrP, or dtBuP). This trend can be seen in Table 4 and Table S3 of the Supporting Information.

For the metal 5,15-disubstituted porphyrins, the degree of nonplanarity (total displacements in Table 4 and Table S3 of the Supporting Information) increases as the substituents become more bulky (phenyl < propyl < isopropyl < *tert*-butyl) as a way of relieving the increasing steric repulsion of the substituents. Furthermore, the contribution from the *ruf* distortion is always larger than the contribution of the *dom* contribution, even though any degree of mixing is symmetry-allowed. The larger contribution from the *ruf* distortion is reasonable because the lowest-frequency mode of B_{1u} symmetry (at 88 cm^{-1}) is softer than that of A_{2u} symmetry (135 cm^{-1}).

As noted, the ratio of *dom* to *ruf* deformations increases as the steric bulk of the substituents increases, a trend shown clearly in Figure 5, which plots the *dom*/*ruf* ratio against the total distortion. This trend can be understood in terms of how easily and how efficiently that steric interaction between the substituents and the adjacent pyrrole rings can be relieved. For the αα 5,15-disubstituted porphyrins, the two symmetry-allowed distortions of the macrocycle, B_{1u} *ruf* and A_{2u} *dom*, can mix in any ratio. For small distortions from planarity, the easiest way to relieve the steric interactions for a *meso*-alkyl porphyrin is to distort along the lowest-frequency normal coordinate of B_{1u} (*ruf*) symmetry. It is a more efficient method of relieving the substituent crowding than doming because it moves the meso carbons and their substituents out of the plane of the macrocycle and away from the C_β atoms of the pyrrole. Thus ruffling is

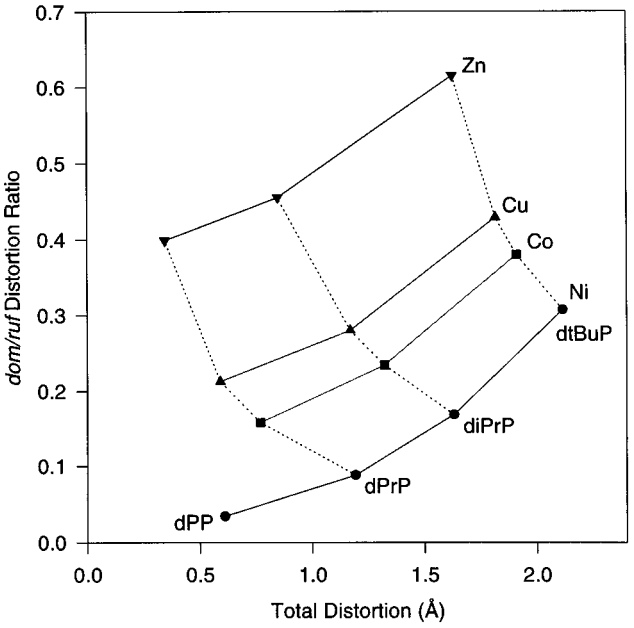

Figure 5. The calculated *dom/ruf* deformation ratio of the αα conformer as a function of total distortion for the series of disubstituted porphyrins.

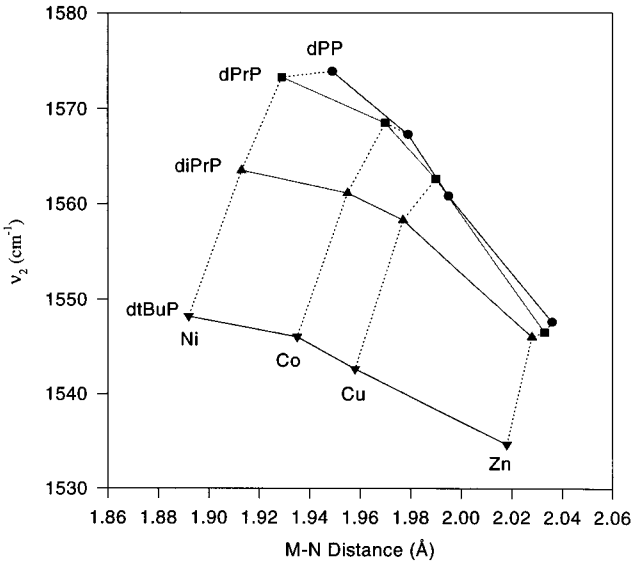

Figure 6. Frequency of the structure-sensitive Raman line ν_2 as a function of metal−nitrogen distance for the series of disubstituted porphyrins.

the predominant contribution to the total distortion for small distortions. However, as the porphyrin becomes more ruffled because of the increasing bulkiness of the substituents, the steric strain in the macrocycle is unnecessarily large. This is because the meso carbons that lack the *tert*-butyl groups are also displaced from the mean plane by the *ruf* distortion. However, by doming, this unnecessary steric strain is relieved, because doming brings the 10- and 20-carbons into a more coplanar configuration with their adjacent pyrrole rings while moving the substituted meso carbons further out of plane.

Comparison of Calculated Structures with the Structural Information Obtained from X-ray Crystallography and Resonance Raman Spectroscopy. The correctness and accuracy of the conformations predicted by molecular mechanics calculations for the 5,15-disubstituted porphyrin were confirmed by crystallographic data. For example, the agreement between the calculated structure and the crystal structures of Cu(dtBuP) is excellent (Figure 2). The predicted increases in total distortion and in the *dom/ruf* ratio as the substituents become bulkier are also confirmed by the crystal structures. For example, the observed *dom/ruf* ratios for the crystal structures of Ni(dPP) (0.08), Ni(diPrP) (0.14), and NidtBuP (0.22) are in reasonable agreement with the calculated ratios of 0.02, 0.14, and 0.27, respectively. In addition, the predicted trend of large metals favoring doming over ruffling is also confirmed by the X-ray structures of Ni(dtBuP) and Cu(dtBuP). The *dom/ruf* distortion ratio is 0.22 for Ni(dtBuP) and 0.38 for Cu(dtBuP), while the corresponding calculated ratios are 0.27 and 0.39 (Table 4). In addition, the *dom/ruf* distortion ratio for the crystal structure of Zn(diPrP)(py) is large [2.7 for *trans*-Zn(diPrP)(py) and 0.41 for *cis*-Zn(diPrP)(py)] in comparison with Ni(diPrP) (0.14). The large values for Zn are partially due to increased metal size and partially due to the coordinated fifth ligand for the Zn complex. Ligation typically favors doming over ruffling for five-coordinate porphyrins.

The predicted increase in nonplanarity for bulkier substituents was further confirmed by shifts to lower frequency for structure-sensitive Raman lines. Figure 6 shows the dependence of the structure-sensitive line ν_2 on the M−N distance for Ni, Co, Cu, and Zn complexes of the 5,15-disubstituted porphyrins. As the porphyrin substituents become more bulky, ν_2 shifts to lower frequency, a trend expected for an increase in macrocycle nonplanarity.[7,8,11a,29]

It has been previously noted that the slope of the correlation between frequency and core size decreases as the porphyrin ring becomes more nonplanar.[11a] The results for the disubstituted porphyrins confirm this observation. The slope of the downshift with metal−nitrogen distance becomes smaller as the bulkiness of the substituents increases and the porphyrin becomes more nonplanar (Figure 6).

The correlation between the frequency of ν_2 and the total nonplanar distortion is shown in Figure S6. This nonlinear dependence has been observed previously.[8] The data shows that the Raman frequencies depend weakly on nonplanar distortion for small deviations from planarity (<1 Å), but vary rapidly for large deviations from planarity (>1 Å).

In some cases, the molecular mechanics calculations predict small energy differences between different conformations of the same metalloporphyrin. The coexistence of multiple conformers can be detected by resonance Raman spectroscopy.[30] One type of structural heterogeneity is the coexistence of both planar and nonplanar forms which occurs for porphyrins with small substituents and small metals. The heterogeneity is a result of the tradeoff between enhanced conjugation in a planar macrocycle and optimal short M−N bond formation in the nonplanar porphyrin. This is the situation in Ni(dPP), where a planar and a *gab* conformer with similar energies are predicted. However, heterogeneity is not predicted for the other metal complexes for which only planar structures are predicted. The resonance Raman spectra of the dPP complexes (Figures S1a and S2a of the Supporting Information) are consistent with these calculations. For Ni(dPP), the ν_2 and ν_8 lines are broad and asymmetric, but the lines become less broad and asymmetric for Co and narrow and symmetric for Cu and Zn.

(29) Czernuszewicz, R. S.; Li, X.-Y.; Spiro, T. G. *J. Am. Chem. Soc.* **1989**, *111*, 7024.
(30) (a) Alden, R. G.; Crawford, B. A.; Doolen, R.; Ondrias, M. R.; Shelnutt, J. A. *J. Am. Chem. Soc.* **1989**, *111*, 2070. (b) Anderson, K. K.; Hobbs, J. D.; Luo, L.; Stanley, K. D.; Quirke, J. M. E.; Shelnutt, J. A. *J. Am. Chem. Soc.* **1993**, *115*, 12346. (c) Jentzen, W. Unger, E.; Karvounis, G.; Shelnutt, J. A.; Dreybrodt, W.; Schweitzer-Stenner, R. *J. Phys. Chem.* **1996**, *100*, 14184.

A second type of structural heterogeneity arises when different orientations of the peripheral substituents give rise to multiple stable conformers of the macrocycle with nearly the same energy. This is the case with the dPrP complexes, for which six stable conformers with similar energies are predicted. This prediction is confirmed by the generally broad and asymmetric shape of ν_2 and ν_8 lines in the Raman spectra of all the dPrP metal complexes (Figures S1b and S2b of the Supporting Information).

For the diPrP complexes, there are four stable conformers (two $\alpha\alpha$ and two $\alpha\beta$) predicted for each metal. However, only the two structurally similar $\alpha\alpha$ conformers are predicted to coexist in solution for Ni, whereas all four conformers may exist in solution for Co, Cu, or Zn (see Results). The Raman results again agree with these predictions, since the Raman spectra of Ni(diPrP) show almost symmetric ν_2 and ν_8 lines, and Co(diPrP), Cu(diPrP), and possibly Zn(diPrP) have asymmetric ν_2 and ν_8 lines (Figures S1c and S2c of the Supporting Information). In the case of the dtBuP complexes, the energies of the calculated structures suggest that irrespective of the size of the central metal atom only the $\alpha\alpha$ conformer will be appreciably populated in solution. In agreement with this prediction, the Raman spectra of the dtBuP complexes (Figure S2d of the Supporting Information) show a narrow and symmetric ν_8 for all metals.

Finally, it should be noted that the apparent doublet seen for the ν_2 line of the dtBuP complexes (Figure S1d of the Supporting Information) is not caused by conformational heterogeneity but by Fermi resonance of ν_2 with another line in the vicinity of ν_2. This was confirmed by preparation of the NidtBuP in which the β-pyrrole positions were selectively deuterated.[8]

Conclusions

The sterically induced nonplanar *gab* distortion of the macrocycle for the series of 5,15-disubstituted porphyrins is a variable combination of *ruf* and *dom* deformations. It can be accurately represented in terms of displacements along the lowest-frequency normal coordinates of B_{1u} and A_{2u} symmetry. The next-higher-frequency normal coordinates of B_{1u} and A_{2u} symmetry are needed to precisely represent the *gab* distortion. The absolute and relative contributions of the normal coordinate deformations to the *gab* distortion depend on the sizes of the metal and substituents. A large metal favors doming over ruffling, reducing the ruffling contribution significantly and increasing the doming contribution slightly. This leads to an overall reduction of degree of nonplanar distortion for large metals. This is explicitly shown by normal-coordinate structural decomposition of the calculated and X-ray structures. Increasing the bulkiness of substituents results in an increasing degree of nonplanar distortion, causing a proportional decrease in the frequencies of the structure-sensitive Raman lines.

Acknowledgment. We thank Dr. J. David Hobbs for helpful discussions and reading of the manuscript.

Supporting Information Available: Selected structural parameters for the calculated $\alpha\beta$-conformers of the 5,15-disubstituted porphyrins (Table S1), the energies of the energy-optimized conformers of the 5,15-disubstituted porphyrins (Table S2), the normal-coordinate structural decomposition results for the $\alpha\alpha$-conformers using the extended basis (Table S3), the normal-coordinate structural decompositions of the $\alpha\beta$-conformers using minimal and extended basis (Tables S4 and S5, respectively), the resonance Raman spectra for the series of 5,15-disubstituted metalloporphyrins in the high-, low-, and middle-frequency regions (Figures S1−3, respectively), comparison of the best fits of the out-of-plane displacements obtained from the X-ray crystal structure and calculated $\alpha\alpha$-conformer of Ni(diPrP) using the minimal and extended basis (Figure S4), comparison of the best fits of the out-of-plane displacements obtained from the X-ray crystal structures of *trans*- and *cis*-Zn(diPrP)(py) (Figure S5), the correlation between the frequency of ν_2 and the total nonplanar distortion for the series of disubstituted metalloporphyrins (Figure S6), the crystal structure of Ni 5,15-diisopropylporphyrin (Figure 57) and its X-ray determination, data collection, and refinement parameters, atomic coordinates, isotropic displacement parameters, bond lengths and angles, and anisotropic displacement parameters (Tables S6−13), the crystal structure of Cu 5,15-di-*tert*-butylporphyrin (Figure S8) and its X-ray determination, data collection, and refinement parameters, atomic coordinates, isotropic displacement parameters, bond lengths and angles, and anisotropic displacement parameters (Tables S1−21), and the two molecules in the X-ray structure of Zn(py) 5,15-diisopropylporphyrin (Figure S9) and its X-ray determination, data collection, and refinement parameters, atomic coordinates, isotropic displacement parameters, bond lengths and angles, and anisotropic displacement parameters (Tables S22−29) (54 pages). Ordering information is given on any current masthead page.

IC970465Z